

# Effect of Field Direction and Field Intensity on Directed Spiral Percolation

Santanu Sinha and S.B. Santra

Department of Physics, Indian Institute of Technology Guwahati,  
Guwahati-781039, Assam, India.  
santra@iitg.ernet.in

March 23, 2024

## Abstract

Directed spiral percolation (DSP) is a new percolation model with crossed external bias fields. Since percolation is a model of disorder, the effect of external bias fields on the properties of disordered systems can be studied numerically using DSP. In DSP, the bias fields are an in-plane directional field ( $E$ ) and a field of rotational nature ( $B$ ) applied perpendicular to the plane of the lattice. The critical properties of DSP clusters are studied here varying the direction of  $E$  field and intensities of both  $E$  and  $B$  fields in 2 dimensions. The system shows interesting and unusual critical behaviour at the percolation threshold. Not only the universality class of DSP model is found to belong in a new universality class than that of other percolation models but also the universality class remains invariant under the variation of  $E$  field direction. Varying the intensities of the  $E$  and  $B$  fields, a crossover from DSP to other percolation models has been studied. A phase diagram of the percolation models is obtained as a function of intensities of the bias fields  $E$  and  $B$ .

**Keywords:** Disordered systems, percolation, external bias fields, anisotropy, critical exponents and universality.

## 1 INTRODUCTION

Recently, a new site percolation model, directed spiral percolation (DSP) [1, 2], was constructed in posing both the directional and rotational constraints simultaneously on the ordinary percolation (OP) [3] model. A new type of anisotropic percolation cluster, different from directed percolation (DP) [4] and spiral percolation (SP) [5], was found in the DSP model. The model showed unusual and interesting critical behaviour at the percolation threshold for the clusters as well as their hulls. It was found that the DSP model belongs to a new universality class than that of other percolation models.

There are certain physical properties of a system needed to be studied in the presence of external biases like electric or magnetic fields. The electric field gives rise to a directional constraint and the magnetic field gives rise to a rotational constraint on the motion of a classical charged particle in a plane when the magnetic field is applied perpendicular to the plane of motion. Since percolation is a model of disorder, Hall effect in disordered systems can be studied using DSP model. Motion of charged particles under crossed electric and magnetic fields in disordered systems is an important field of study in recent time [6, 7].

In this paper, the DSP model is studied on the square and triangular lattices in 2-dimensions (2D) varying the field intensities and the direction of the fields. As the direction of a field changes, the number of components of the field on a lattice also changes. The universality class of DSP model has been verified for different number of field components. It is found that the universality class of DSP is independent of the field directions or the number of components of the directed field. As the intensities of the fields change, the DSP model is expected to change to OP, DP or SP models at the appropriate field intensities. Varying the external field intensities, crossover from DSP to other percolation models has been studied. A complete phase diagram is obtained for the percolation models studying the DSP model under variable field intensities.

Below, the DSP model will be developed under variable field directions and variable field intensities. The effect of change of field direction will be discussed first. Intensity effect will be considered later.

## 2 D SP Model under Variable Field Direction

The D SP model for different field orientations is constructed on the square and triangular lattices in 2D. The particles are considered to be classical charged particles to form percolation clusters under external bias fields. Two external bias fields perpendicular to each other are present in the model. An in-plane electric field  $E$  gives rise to a directional constraint and a magnetic field  $B$  perpendicular to the plane of the lattice, directed into the plane, gives rise to clockwise rotational constraint to the occupation of a lattice site by a particle. A single cluster growth Monte Carlo (MC) algorithm to generate D SP clusters under different field orientations will be described here. In this algorithm, the central site of the lattice is occupied with unit probability. All the nearest neighbors of the central site can be occupied with equal probability  $p$  in the first time step. As soon as a site is occupied, the direction from which it was occupied is assigned to it. Once the directional  $E$  field is fixed, the empty nearest neighbours in that fixed direction in space are accessible to occupation due to the directional constraint. In contrary, for a given  $B$  field direction, the empty nearest neighbours accessible to occupation are in the forward direction or in a rotational direction, clockwise here, with respect to the direction of occupation of the present site. Since the forward and rotational directions depend on the direction of occupation of the present site, then the rotational constraint is not fixed in space. First, a list of empty nearest neighbours eligible for occupation in the next MC time steps is prepared. Selection of eligible sites on the square lattice is illustrated in Figs.1 (a) and 1 (b) and on the triangular lattice it is illustrated in Figs.1 (c) and 1 (d). On the square lattice, the  $E$  field is in the horizontal direction in Fig.1 (a) and it is along the upper left to the lower right diagonal of the lattice in Fig.1 (b). On the triangular lattice, the  $E$  field is horizontal in the Fig.1 (c) and in Fig.1 (d), the  $E$  field is from upper left to the lower right corner making an angle  $30^\circ$  with the horizontal, a semi-diagonal field ( $E$  field along  $60^\circ$  with the horizontal on the triangular lattice is not considered because it will lead to anisotropic current distribution). The presence of  $E$  field is shown by the long arrows. The  $B$  field is always perpendicular to the plane of the lattice and directed into the plane as indicated by the encircled dots. The descriptions given below are valid for all field configurations given in Fig.1. The black circles represent the occupied sites and the open circles represent the empty sites. The direction from which the central site is occupied is represented by a short thick arrow. In Fig.1, the central site is always occupied from site 2. The eligible empty sites for occupation due to  $E$  field are indicated by dotted arrows and thin solid arrows indicate the same due to  $B$  field. The number of eligible empty sites for occupation due to  $B$  field depends on the lattice structure. There are two such sites on the square lattice, as shown in Fig.1 (a) and 1 (b), whereas there are three such sites available on the triangular lattice, as shown in Fig.1 (c) and 1 (d) by thin arrows. If the direction of  $B$  field is changed from 'into the plane' to 'out of the plane' only the sense of rotational constraint will be changed but the number of eligible empty sites for occupation will remain the same. However, the number of eligible empty sites for occupation due to  $E$  field depends on the direction of the  $E$  field. There is one such site for the horizontal  $E$  field on both the lattices whereas there are two such sites for the diagonal  $E$  field on the square lattice and for the semi-diagonal  $E$  field on the triangular lattice. Two eligible sites for occupation in case of diagonal or semi-diagonal  $E$  field orientation is the consequence of two equal components of the  $E$  field along those two nearest neighbours, as indicated by two dotted arrows in Fig.1 (b) and Fig.1 (d).

After selecting the eligible empty sites for occupation, they are occupied with probability  $p$ . The coordinate of an occupied site in a cluster is denoted by  $(x, y)$ . Periodic boundary conditions are applied in both directions and the coordinates of the occupied sites are adjusted accordingly whenever the boundary is crossed. At each time step the span of the cluster in the  $x$  and  $y$  directions  $L_x = x_{max} - x_{min}$  and  $L_y = y_{max} - y_{min}$  are determined. If either  $L_x$  or  $L_y$  of a cluster is found greater than or equal to  $L$ , the system size, the cluster is then considered as a spanning cluster. The critical percolation probability  $p_c$  is the maximum probability below which there is no spanning cluster appears and at  $p = p_c$  a spanning cluster appears for the first time in the system.

## 3 Effect of Field Direction

The critical properties of D SP model is studied numerically under diagonal  $E$  field on the square lattice and semi-diagonal  $E$  field on the triangular lattice. For the diagonal or semi-diagonal  $E$  field orientation, there are two components of the field on both the lattices along which the lattice sites could be occupied. Results obtained here are compared with that of already obtained results under horizontal  $E$  field orientations, single component of  $E$  field, on the respective lattices [1, 2]. Lattice size is varied from  $L = 2^7$  to  $2^{11}$  in multiple of 2. Firstly the percolation thresholds ( $p_c$ s) are determined for each field configuration on a given lattice. The cluster related quantities are

then evaluated at their respective  $p_c$ s. Each data point is averaged over  $N_{\text{tot}} = 5 \times 10^4$  clusters.

### 3.1 Percolation threshold

Percolation threshold  $p_c$  is the maximum site occupation probability at which a spanning cluster appears for the first time in the system.  $p_c$ s are determined here for the diagonal  $E$  field on the square lattice and semi-diagonal  $E$  field on the triangular lattice in the presence of a crossed  $B$  field. The probability to have a spanning cluster is given by  $P_{\text{sp}} = n_{\text{sp}}/N_{\text{tot}}$  where  $n_{\text{sp}}$  is the number of spanning clusters out of  $N_{\text{tot}}$  clusters generated. The value of  $p_c$  for a given system size  $L$  and a given  $E$  and  $B$  field configuration is determined from the maximum slope of the curve  $P_{\text{sp}}$  versus  $p$ . Generally,  $p_c$  depends on  $L$  for finite systems. The value of  $p_c$  is then determined as function of  $L$  for a given lattice and field configuration. Data are then extrapolated to  $L \rightarrow \infty$ . In Fig 2,  $p_c(L)$  is plotted against the inverse system size  $1/L$  for different field configurations on both the lattices. Circles represent  $p_c$ s for the diagonal  $E$  field on the square lattice and diamonds represent the same for the semi-diagonal  $E$  field on the triangular lattice. The  $p_c$ s of infinite systems are identified in the  $1/L \rightarrow 0$  limit and marked by crosses. It is found that  $p_c = 0.619$  for diagonal  $E$  field on the square lattice and  $0.545$  for semi-diagonal  $E$  field on the triangular lattice respectively. For the sake of comparison,  $p_c$ s for the horizontal  $E$  field configuration on both the lattices for different system size are also plotted in the same figure. The squares represent data for the horizontal  $E$  field on the square lattice and triangles represent the same for the horizontal  $E$  field on the triangular lattice. It was already obtained that  $p_c = 0.655$  [1] and  $0.570$  [2] for the horizontal  $E$  field on the square and triangular lattices respectively as it is also shown here. As usual, the value of  $p_c$  depends on the type of lattice as well as on the field situation. If the lattice structure is changed, the number of components of rotational constraint changes. If the direction of  $E$  field changes on a lattice, the number of components of directional constraint changes. The value of  $p_c$  is decreased if the number of field components is increased either by the rotational constraint or by the directional constraint. It is expected, because, the clusters can grow rapidly if the number of field components are higher in a given lattice.

### 3.2 Effective field and Spanning clusters

Typical spanning clusters at  $p = p_c$  for different field configurations on the square and triangular lattices of size  $L = 2^8$  are shown in Fig.3. Spanning clusters generated on the square lattice for the horizontal and diagonal  $E$  field orientations are represented in Fig.3 (a) and in Fig.3 (b) respectively. Fig.3 (c) and Fig.3 (d) represent the spanning clusters on the triangular lattice for the horizontal and semi-diagonal (30° with the horizontal)  $E$  field orientations respectively. The  $B$  field is always perpendicular to the  $E$  field and directed into the plane of the lattice as shown by encircled dots. The black dots indicate the external boundary of the cluster and the gray dots represent the interior of the cluster. It can be seen that the clusters are highly rarefied, anisotropic and have chiral dangling ends. Interestingly, the elongation of the clusters are not along the applied  $E$  field. This is due to the generation of the Hall field  $E_H$  perpendicular to the applied fields  $E$  and  $B$ . As a result, an effective field  $E_e$  develops in the system and the elongation of the clusters are along the effective field. Since the direction of the effective field depends on the direction of the applied  $E$  field, the orientation of the cluster grown then depends on the direction of the applied  $E$  field. However, the clusters are not merely DP clusters along the effective field. Because, the presence of the rotational  $B$  field gives rise to chiral dangling ends at the boundary which has its own critical behaviour [8]. It is important to notice that the clusters are less anisotropic and more compact on the triangular lattice than on the square lattice. This is due to the extra flexibility given in the  $B$  field on the triangular lattice. However, the clusters look indifferent under different  $E$  field orientations on a given lattice except their direction of growth.

### 3.3 Fractal dimension

The fractal dimension  $d_f$  of the infinite or spanning clusters are determined by the box counting method. The number of boxes  $N_B(\ell)$  grows with the box size  $\ell$  as  $N_B(\ell) \propto \ell^{-d_f}$  where  $d_f$  is the fractal dimension. In Fig.4,  $N_B(\ell)$  is plotted against the box size  $\ell$  for the square (a) and triangular (b) lattices for all  $E$  field orientations. On the square lattice, the fractal dimensions are found as  $d_f = 1.733 \pm 0.005$  for the horizontal  $E$  field and  $d_f = 1.732 \pm 0.006$  for the diagonal  $E$  field. Similarly on the triangular lattice, it is found that  $d_f = 1.775 \pm 0.004$  for the horizontal  $E$  field and  $d_f = 1.777 \pm 0.005$  for the semi-diagonal  $E$  field. The error is due to the least square fit. These estimates are also confirmed by finite size (FS) analysis. In FS analysis,  $d_f$  is determined employing

$S_1 \propto L^{d_f}$ , where  $S_1$  is the mass of the spanning cluster. The FS estimates are  $d_f = 1.72 \pm 0.02$  on the square lattice and  $d_f = 1.81 \pm 0.02$  on the triangular lattice for the diagonal and semi-diagonal E-eld respectively. It is interesting to notice that the change in the direction of the E-eld has no effect on the values of  $d_f$  on both the lattices. However, the values of  $d_f$  are different on the square and triangular lattices as already reported in Ref.[2]. It was already found that  $d_f$  is higher on the triangular lattice than that of on the square lattice consistent with the observation that the spanning clusters are more compact on the triangular lattice than on the square lattice. For a given E-eld direction, the D SP model on these two lattices differ only by an extra rotational direction due to B-eld on the triangular lattice than that on the square lattice. The change in  $d_f$  on these two lattices is then only due to the different number of branching of the rotational constraint due to the B-eld in the presence of a directional eld. The extra flexibility of the rotational constraint allows the clusters to penetrate more and more into itself on the triangular lattice than on the square lattice. As a result, the infinite clusters are less rarefied on the triangular lattice than on the square lattice. Since the clusters grow along the effective eld direction, the orientation of the clusters is only changing with the orientation of the E-eld as the effective eld direction is changing. Note that, the value of  $d_f$  obtained here is not only different from other percolation models but also smallest among that of OP (91=48[9]), DP (1.765[10]) and SP (1.969[11]). The spanning clusters are then most rarefied in D SP. Since  $d_f$  obtained in D SP is different from that of DP clusters, it could be inferred that the D SP clusters are just not DP clusters along the effective eld. The D SP clusters then should have its own critical behaviour at the percolation threshold as it is already observed [1]. It is now important to check the effect of E-eld direction on the other critical exponents.

### 3.4 Critical exponents and Scaling relations

The values of some of the critical exponents are estimated and the scaling relations among them are verified in this section. A full scaling theory of D SP model is given in Ref.[1]. The cluster size distribution is defined as  $P_s(p) = N_s/N_{tot}$  where  $N_s$  is the number of  $s$ -sited clusters in a total of  $N_{tot}$  clusters generated. Since the origin of a cluster is occupied with unit probability, the scaling function form of the cluster size distribution is assumed as

$$P_s(p) = s^{-\alpha-1} f[s^{-\beta}(p - p_c)] \quad (1)$$

where  $\alpha$  and  $\beta$  are two exponents. The form of  $P_s(p)$  has already been verified and found appropriate for D SP [1, 2]. In order to verify the scaling relations among the critical exponents, the average cluster size,  $\bar{s} = \sum_s s P_s(p)$ , and two other higher moments,  $\bar{s}^2 = \sum_s s^2 P_s(p)$  and  $\bar{s}^3 = \sum_s s^3 P_s(p)$ , of the cluster size distribution  $P_s(p)$  are measured generating infinite clusters below  $p_c$ . E-eld is applied diagonally on the square lattice and semi-diagonally on the triangular lattice in the presence of a crossed B-eld directed into the plane of the lattice. For a system size  $L = 2^{11}$ ,  $\bar{s}$  is plotted against  $p - p_c$  for diagonal E-eld on the square lattice (circles) in Fig.5 (a) and for semi-diagonal E-eld on the triangular lattice (diamond) in Fig.5 (b). Data corresponding to horizontal E-eld on the square (squares) [1] and triangular (triangles) [2] lattices are also plotted in the respective figures for comparison with the present data. It can be seen from Fig.5 that not only the absolute magnitude of the average cluster size but also the scaling of  $\bar{s}$  with  $p - p_c$  remains independent of the E-eld orientation on both the lattices. The value of  $\beta$  is found  $1.87 \pm 0.02$  for the diagonal E-eld whereas for the horizontal E-eld it was  $1.85 \pm 0.02$  on the square lattice. Thus, the value of the exponent  $\beta$  is within error bar for both the E-eld orientations on the square lattice. A similar result is also obtained on the triangular lattice. It is found that  $\beta = 2.00 \pm 0.02$  for semi-diagonal E-eld whereas it was  $1.98 \pm 0.02$  for the horizontal E-eld on the triangular lattice. The errors quoted here include the least square fit error and the change in  $\beta$  with  $p_c$  for  $p_c = 0.0005$ . Similarly, estimates of the critical exponents  $\alpha$  and  $\nu$  related to the higher moments of the cluster size distributions are also obtained. The observations are listed in Table 1. It can be seen that the values of all the critical exponents are very close and within error bars for different E-eld orientations on a given lattice. Finite size analysis of these critical exponents  $\alpha$ ,  $\beta$ , and  $\nu$  have also been made. The values of  $\alpha$ ,  $\beta$ , and  $\nu$  are determined on different system size  $L$ . In Fig.6, the exponents are plotted against the system size  $L$ . The extrapolated values of the exponents in the  $L \rightarrow \infty$  limit are marked by crosses. As expected, the finite size estimates of  $\alpha$ ,  $\beta$ , and  $\nu$  are converging to the Monte Carlo results on both the lattices as  $L \rightarrow \infty$ . It is interesting to notice that the exponent values are close and within error bars for different E-eld orientation on a given lattice although they are significantly different (out of error bars) on the square and triangular lattices. The exponents  $\alpha$ ,  $\beta$ ,

and satisfy a scaling relation  $\nu = 2$ . The scaling relation has already been verified in Ref.[1] and [2] for horizontal E field and found holds true. The same scaling relation has also been tested with the obtained values of the exponents for diagonal/semi-diagonal orientations of E field and it is satisfied within error bars irrespective of E field orientations on both the lattices.

Since the clusters generated here are anisotropic, there are then two connectivity lengths:  $\nu_k$  along the elongation of the cluster and  $\nu_\perp$  along the normal to the elongation. They are defined as  $\nu_k = 2 \frac{0}{s} R_k^2(s) s P_s(p) = \frac{0}{s} s P_s(p)$  and  $\nu_\perp = 2 \frac{0}{s} R_\perp^2(s) s P_s(p) = \frac{0}{s} s P_s(p)$  where  $R_k(s)$  and  $R_\perp(s)$  are the two radii of gyration with respect to two principal axes. The connectivity lengths,  $\nu_k \sim |p - p_c|^{-\nu_k}$  and  $\nu_\perp \sim |p - p_c|^{-\nu_\perp}$  diverge with two different critical exponents  $\nu_k$  and  $\nu_\perp$  as  $p \rightarrow p_c$ . The scaling behaviour of  $\nu_k$  and  $\nu_\perp$  are studied as function of  $p$  below  $p_c$  for diagonal E field on the square lattice and for semi-diagonal E field on the triangular lattice. For lattice size  $L = 2^{11}$ ,  $\nu_k$  and  $\nu_\perp$  are plotted against  $|p - p_c|$  in Fig.7 (a) for the square lattice and in Fig.7 (b) for the triangular lattice for different E field orientations. The exponents  $\nu_k$  and  $\nu_\perp$  are obtained as  $1.34 \pm 0.02$  and  $1.13 \pm 0.02$  respectively for diagonal E field on the square lattice (circles). On the triangular lattice, they are found as  $\nu_k = 1.37 \pm 0.02$  and  $\nu_\perp = 1.24 \pm 0.02$  for the semi-diagonal E field (diamonds). Data for the horizontal E field are indicated by squares for the square lattice and by triangles for the triangular lattice. The values of  $\nu_k$  and  $\nu_\perp$  are found within error bars for different E field orientations on both the lattices, see Table 1. The errors quoted here are the least square fit errors. Finite size estimates of these exponents are also made and it is found that they are consistent with that of the MC results. The exponent  $\nu_k$  is almost same on the square and triangular lattices whereas  $\nu_\perp$  on the triangular lattice is little higher than that of the square lattice value.  $\nu = \nu_k \nu_\perp$  is  $0.21$  for DSP on the square lattice whereas it is  $0.64$  in DP [12]. The DSP clusters are then less anisotropic than that of DP clusters. This observation remains unchanged even if the direction of the effective field, along which the clusters grow, is changed. It is also noticed that the critical behaviour of the connectivity length  $\nu_k$  along the elongation of the cluster is similar to that of the connectivity length of ordinary percolation. The value of  $\nu_k$  is almost equal to  $\nu_{OP} = 4/3$  [9]. This is in good agreement with a recent study of magnetoresistance of a three-component composites of metallic In by Barabash et al [13]. It is found that the hyperscaling relations  $2 - 3 = (d - 1)\nu_\perp + \nu_k$  and  $(d - d_f)\nu_\perp = 2$  are satisfied on the square lattice within error bars whereas they are satisfied marginally on the triangular lattice. It is already known that the hyperscaling is violated in DP [14].

The results obtained for different E field orientations on the square and triangular lattices are summarized in Table 1. Comparing the data given in Table 1 it can be concluded that the values of the critical exponents and the scaling relations among them are independent of E field orientation or the number of components of E field irrespective of lattice structure. The direction of E field is only able to change the orientation of the clusters and not the critical properties. However, it has already been observed that the values of the critical exponents obtained in DSP model are not only different from that of the other percolation models but also are significantly different on the square and triangular lattices in 2D. It is already reported in Ref.[2] as a breakdown of universality between the square and triangular lattices. Microscopically, the DSP model on the square and triangular lattices differs only by an extra rotational direction due to B field on the triangular lattice than that on the square lattice for a given E orientation. The values of the critical exponents then depend on the number of branching due to the rotational field B but do not depend on the number of branching due to the directional field E. By reducing the number of branching of B field from three to two on the triangular lattice and keeping E field horizontal, an artificial model has been created and the critical exponents are re-estimated. The values of the critical exponents for this particular field combination are obtained as:  $d_f = 1.730 \pm 0.005$ ,  $\nu = 1.87 \pm 0.01$ ,  $\nu_k = 4.08 \pm 0.04$  and  $\nu_\perp = 6.34 \pm 0.08$ . Remarkably, the values of  $d_f$  and other critical exponents are found within error bars of that of the square lattice with horizontal E field and the universality holds. It should be mentioned here that no breakdown of universality was observed in SP [11], percolation under only rotational constraint, between the square and triangular lattices. In DSP model, the presence of the directional constraint E on top of the rotational constraint B may increase the number of spiral lattice trees. Since the spiral lattice trees [15] as well as the spiral self avoiding walks [16] have different scaling behaviour on the square and triangular lattices, the higher number of tree like structures in the clusters generated can induced a non-trivial effect on the critical properties of DSP at the percolation threshold and consequently the discrepancy in the exponent values on the two lattices could occur.

Though there is a breakdown of universality in the cluster property of the DSP model on the

square and triangular lattices, it was already observed that the universality holds true for their hull (external perimeter) properties between the square and triangular lattices [17]. The hull properties are also verified here by changing the applied E field direction and it is found that the hull properties are independent of the E field orientations.

## 4 D SP Model under Variable Field Intensity

So far, the D SP model has been investigated under constant external field intensities. It is also useful to understand the properties of disordered system as function of the field intensity. The intensities  $E$  and  $B$  of the external fields can vary here from 0 to 1. It may be noted that for certain extreme values of the intensities  $E$  and  $B$ , the percolation model has four different varieties, D SP, DP, SP and OP. D SP corresponds to  $E = 1, B = 1$ ; DP corresponds to  $E = 1, B = 0$ ; SP corresponds to  $E = 0, B = 1$  and OP corresponds to  $E = 0, B = 0$ . Thus, a complete phase diagram can also be obtained by studying the D SP model under variable field intensities between one and zero. If the field intensities are changed continuously from (1;1) to (0;0) keeping  $E = B$ , it is expected to have a phase change from D SP to OP. Similarly, a phase change from D SP to SP can be obtained by changing  $E$  from 1 to 0 keeping  $B = 1$  and phase change from D SP to DP can be obtained by changing  $B$  from 1 to 0 keeping  $E = 1$ . In order to study the effect of intensities of the external applied fields, one needs to generate percolation clusters under variable field intensities and characterize their geometrical properties at the percolation threshold. The intensity dependent percolation cluster could be generated by selecting nearest neighbours of an occupied site with appropriate probabilities, function of field intensities. To demonstrate the model, a square lattice of size  $L$  is considered. The E field is applied diagonally and the B field is applied perpendicular to the E field and directed into the plane of the lattice as shown in Fig.1 (b). However, the results of this particular field configuration should be valid for all other field configurations. In order to occupy a site in the presence of external fields, a list of eligible sites for occupation is prepared first. The field intensities play role in the preparation of the list of eligible sites. If the field intensities are either  $E = 1$  or  $B = 1$  or both  $E = B = 1$ , the sites only in the favourable directions, defined by the directional and rotational constraints, are eligible for occupation. Sites in other directions are not considered for occupation in all three constrained percolation models D SP, DP and SP. The sites in the favourable directions of the fields are selected with probabilities proportional to the field intensities. If the field intensities are less than one, the sites in unfavourable directions of the fields will also be eligible for occupation due to scattering. A scattering field  $S$  is then introduced in the model. Sites in unfavourable directions are selected for occupation with probability  $S$  and it is defined as

$$S = (1 - E) (1 - B); \quad (2)$$

Notice that  $S = 0$  in all three cases:  $E = 1, B = 1$  and  $E = B = 1$ . That means there is no scattering and consequently no sites in unfavourable directions are eligible for occupation as in the case of DP, SP or D SP. On the other hand, when  $E$  and  $B$  both are equal to zero then  $S = 1$ . There will be then no favourable direction. All empty nearest neighbours of an occupied site on the square lattice are selected with unit probability for occupation. The situation corresponds to OP. Thus, a change of phase from D SP to OP, DP or SP will be possible by changing  $E$  and  $B$  continuously. As soon as the list of eligible sites is prepared they are then occupied with percolation probability  $p$ . Below, the critical properties of D SP clusters are studied varying intensity of  $E$  and  $B$  fields. For each value of  $E$  and  $B$ , the percolation threshold  $p_c$  is determined. Data are averaged over  $10^5$  clusters for each field intensity.

## 5 Effect of field intensity

The field intensities are changed in three different ways. First,  $E$  and  $B$  are changed from (1;1) to (0;0) keeping  $E = B$  and accordingly D SP is expected to change over to OP. The corresponding data will be represented by circles. Second, keeping  $B = 1$ ,  $E$  is changed from 1 to 0, then D SP should change to SP. These data are represented by squares. Third, keeping  $E = 1$ ,  $B$  is changed from 1 to 0, thus DP will be reached from D SP. Triangles represent the corresponding data. Percolation threshold  $p_c$ , at which a spanning cluster appears for the first time in the system, has been calculated as function of the field intensities  $E$  and  $B$ . Following the same procedure of section 3,  $p_c$ s are identified as the percolation probability  $p$  corresponding to the maximum slope of the plot of spanning probability  $P_{sp}$  against  $p$ . In Fig.8, the values of  $p_c$ s are plotted against  $E$  and  $B$  for a square lattice of size  $L = 1024$ . Each  $p_c$  has been determined generating  $10^5$  spanning

clusters. It can be seen that as  $E$  and  $B$  goes to zero  $p_c$  coincides with that of OP. Similarly,  $p_c$  for DP and SP are also obtained for  $E = 1; B = 0$  and  $E = 0; B = 1$  respectively.

The percolation clusters are isotropic for OP and SP whereas they are anisotropic in the case of DP and DSP. For anisotropic clusters, there are two connectivity lengths  $\xi_\parallel$  and  $\xi_\perp$  and for isotropic clusters there is only one connectivity length. Since  $\xi_\parallel$  and  $\xi_\perp$  diverge with two critical exponents  $\nu_\parallel$  and  $\nu_\perp$  respectively as  $p \rightarrow p_c$ , the ratio of two connectivity lengths  $\xi_\parallel/\xi_\perp$  should diverge as  $(p - p_c)^{-\Delta}$  where  $\Delta = \nu_\parallel - \nu_\perp$ . For isotropic clusters,  $\xi_\parallel$  is equal to  $\xi_\perp$  since the clusters grow equally in all directions. Thus,  $\Delta$  is zero for OP and SP clusters and  $\Delta$  is finite for anisotropic clusters of DP and DSP. In DSP,  $\Delta$  is approximately 0.21 [1] whereas in DP, it is approximately 0.64 [12]. The values of the connectivity exponents  $\nu_\parallel$  and  $\nu_\perp$  are determined for different values of  $E$  and  $B$ . In Fig.9,  $\Delta$  is plotted against  $E$  and  $B$ . As the field intensities are taken to  $E = 0$  and  $B = 0$  or  $E = 0$  and  $B = 1$  corresponding to OP and SP models the value of  $\Delta$  continuously goes to zero. As the field intensities are taken to  $E = 1$  and  $B = 0$  corresponding to the DP model, the value of  $\Delta$  approaches to 0.64 as it is expected for DP. Not only the difference but also the absolute value of the connectivity exponent matches with the respective percolation models. Thus, there is a smooth crossover from DSP to OP, DP and SP at the appropriate values of  $E$  and  $B$  as they are changed continuously.

In order to determine other critical properties, fractal dimension  $d_f$  of the spanning clusters and average cluster size exponent  $\tau$  are also determined.  $d_f$  is plotted in Fig.10 and  $\tau$  is plotted in Fig.11 against  $E$  and  $B$ . The value of  $d_f$  in different percolation models are:  $d_f(OP) = 1.896$  [9],  $d_f(DP) = 1.765$  [10],  $d_f(SP) = 1.957$  [11] and  $d_f(DSP) = 1.733$  [1]. The values of  $d_f$  for OP, DP and SP are marked by crosses in Fig.10. It can be seen that the value of  $d_f$  changes continuously and approaches to the expected values of  $d_f$  of the respective percolation models as the intensities of  $E$  and  $B$  are changed appropriately. In Fig.11, the values of  $\tau$  of different percolation models are also indicated by crosses,  $\tau(OP) = 43.18$  [9],  $\tau(DP) = 22.772$  [10],  $\tau(SP) = 2.19$  [11] and  $\tau(DSP) = 1.85$  [1]. Similar to the fractal dimension, the value of the critical exponent  $\tau$  is also changing continuously to that of the other percolation models as the intensities of  $E$  and  $B$  are changed appropriately. However, for most of the  $E$  and  $B$  values, the values of  $d_f$  and other critical exponents are found close to that of DSP. It could also be noticed that in the presence of small field intensities of  $E$  or  $B$ , the universality class of OP is changed. Similarly for DP and SP, a small intensity of the other field is able to change the universality class of the models to that of DSP. This is a new and important observation.

A phase diagram for percolation models under external bias fields now can be plotted in the space of directional ( $E$ ) and rotational ( $B$ ) bias fields. Different percolation models are identified on the  $E-B$  space by black circles in Fig.12. Each point in this space corresponds to a second order phase transition point. The thick lines from left lower to right upper diagonal and parallel to the  $E$  and  $B$  axes of the phase diagram represent lines of second order phase transition points. The two ends of the diagonal line correspond to OP and DSP. The line parallel to  $E$  connects SP and DSP whereas the line parallel to  $B$  connects DP and DSP. The dotted lines define the regions of DP and SP as indicated. DSP model then can be considered as the most generalized model of percolation under external bias fields whose different limiting situations correspond to other percolation models like OP, DP or SP.

## 6 Summary

The directed spiral percolation model has been studied varying the applied field directions and their intensities on the square and triangular lattices in 2D. The critical properties of the cluster related quantities in this model were already found very different from the other percolation models like OP, DP and SP and accordingly DSP belongs to a new universality class. It is found here that the critical properties as well as the universality class of the DSP clusters remain invariant on the directions of the applied  $E$  and  $B$  fields. Change of  $E$  field direction corresponds to the change in the number of components of the  $E$  field on both the lattices. However, this is not the case for  $B$  field. Change in the number of components in the  $E$  field corresponds to the change in orientations of the clusters only whereas change in the number of components in the  $B$  field corresponds to the change in the universality class of DSP. Changing the intensity of the applied fields, a smooth crossover from DSP to OP, DP and SP is observed. A phase diagram is obtained for the percolation models under external bias fields. OP, DP or SP could be obtained as a limiting situation of DSP by changing the field intensities. The DSP model then can be considered as a most general model of percolation under external bias fields. The model will be applicable to the physical situations

where crossed directional and rotational force fields are present in disordered systems.

Acknowledgment: SS thanks CSIR, India for financial support.

## References

- [1] S.B. Santra, Eur. Phys. J. B 33, 75 (2003); Int. J. Mod. Phys. B 17, 5555 (2003).
- [2] S. Sinha and S.B. Santra, Eur. Phys. J. B 39, 513 (2004).
- [3] D. Stauffer and A. Aharony, Introduction to Percolation Theory, 2nd edition, (Taylor and Francis, London, 1994).
- [4] H. Heinrichsen, Adv. Phys. 49, 815 (2000) and references therein.
- [5] P. Ray and I. Bose, J. Phys. A 21, 555 (1988); S.B. Santra and I. Bose, J. Phys. A 24, 2367 (1991).
- [6] S.B. Santra and W.A. Seitz, Int. J. Mod. Phys. C 11, 1357 (2000).
- [7] R. Burioni, D. Cassi, G. Giusiano and S. Regina, Phys. Rev. E 67, 016116 (2003).
- [8] S.B. Santra and I. Bose, J. Phys. A 26, 3963 (1993).
- [9] M.P.M. den Nijs, J. Phys. A 12, 1857 (1977); B. Nienhuis, J. Phys. A 15, 199 (1982).
- [10] B. Hede, J. Kertesz and T. Vicsek, J. Stat. Phys. 64, 829 (1991).
- [11] S.B. Santra and I. Bose, J. Phys. A 25, 1105 (1992).
- [12] J.W. Essam, K. DeBell and J. Adler, Phys. Rev. B 33, 1982 (1986); J.W. Essam, A.J. Guttmann and K. DeBell, J. Phys. A 21, 3815 (1988).
- [13] S.V. Barabash, D.J. Bergman and D. Stroud, Phys. Rev. B 64, 174419 (2001).
- [14] M. Henkel and V. Privman, Phys. Rev. Lett. 65, 1777 (1990).
- [15] S.B. Santra, J. Phys. I France 5, 1573 (1995).
- [16] H.J.W. Blöte and H.J. Hilhorst, J. Phys. A 17, L111 (1984); K.Y. Lin, J. Phys. A 18, L145 (1985).
- [17] S. Sinha and S.B. Santra, Int. J. Mod. Phys. C 16, 1251 (2005).



Lattice Type	E field orientation	$d_f$								$k$		$\tau$	
Square:	Horizontal[1]:	1:733	0:005	1:85	0:01	4:01	0:04	6:21	0:08	1:33	0:01	1:12	0:03
		1:72	0:02 (FS)										
	Diagonal:	1:732	0:006	1:87	0:01	4:04	0:04	6:24	0:08	1:34	0:02	1:13	0:02
		1:72	0:02 (FS)										
Triangular:	Horizontal[2]:	1:775	0:004	1:98	0:02	4:30	0:04	6:66	0:08	1:36	0:02	1:23	0:02
		1:80	0:03 (FS)										
	Semi-diagonal:	1:777	0:005	2:00	0:02	4:33	0:04	6:71	0:08	1:37	0:02	1:24	0:02
		1:81	0:02 (FS)										

Table 1: Numerical estimates of the critical exponents and the fractal dimension measured for the DSP clusters on the square and triangular lattices for different E field orientations. The values of the critical exponents and the fractal dimension are found independent of the orientation of E field on both the lattices.

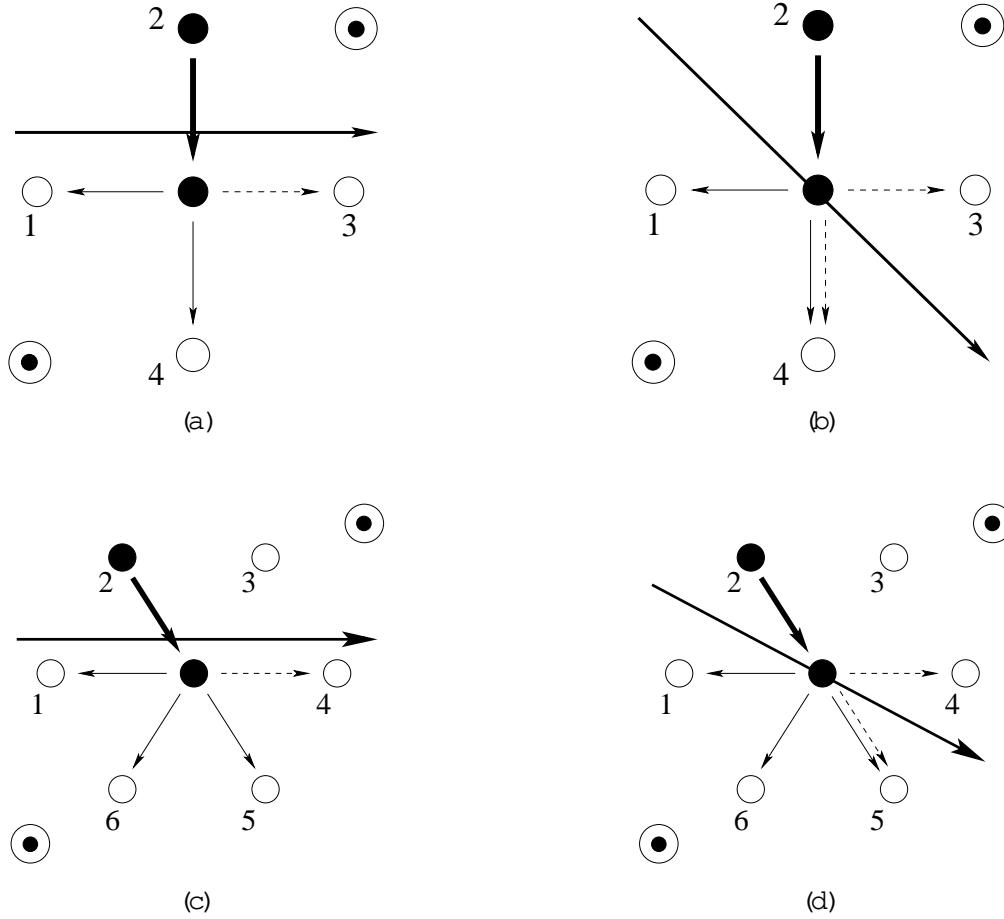


Figure 1: Selection of empty nearest neighbors for occupation in a MC time step on the square (a, b) and triangular (c, d) lattices. Black circles are the occupied sites and the open circles are the empty sites. Thick long arrows represent directional constraint ( $E$ ). The clockwise rotational constraint ( $B$ ) is shown by encircled dots. The central site is occupied from site 2 and shown by short thick arrows. The eligible sites for occupation due to  $E$ -field are shown by dotted arrows and thin solid arrows indicate the same due to  $B$ -field on both the lattices.

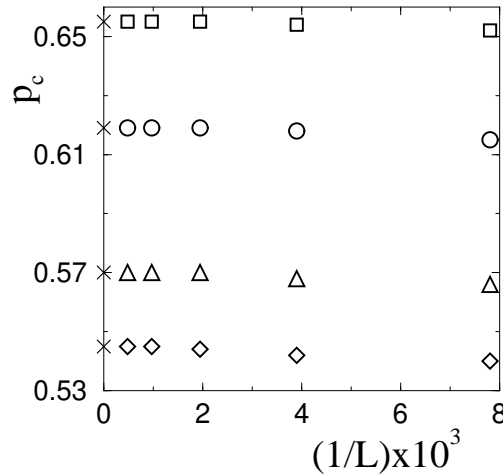


Figure 2: Plot of critical probability  $p_c(L)$  versus  $1/L$  for different  $E$ -field orientations. The symbols are: (2) for the horizontal  $E$  and ( ) for the diagonal  $E$ -field on the square lattice, (4) for the horizontal  $E$  and (3) for the diagonal  $E$ -field on the triangular lattice. The values of  $p_c(L)$  are extrapolated to  $L \rightarrow \infty$  and  $p_c$  for infinite systems are indicated by crosses.

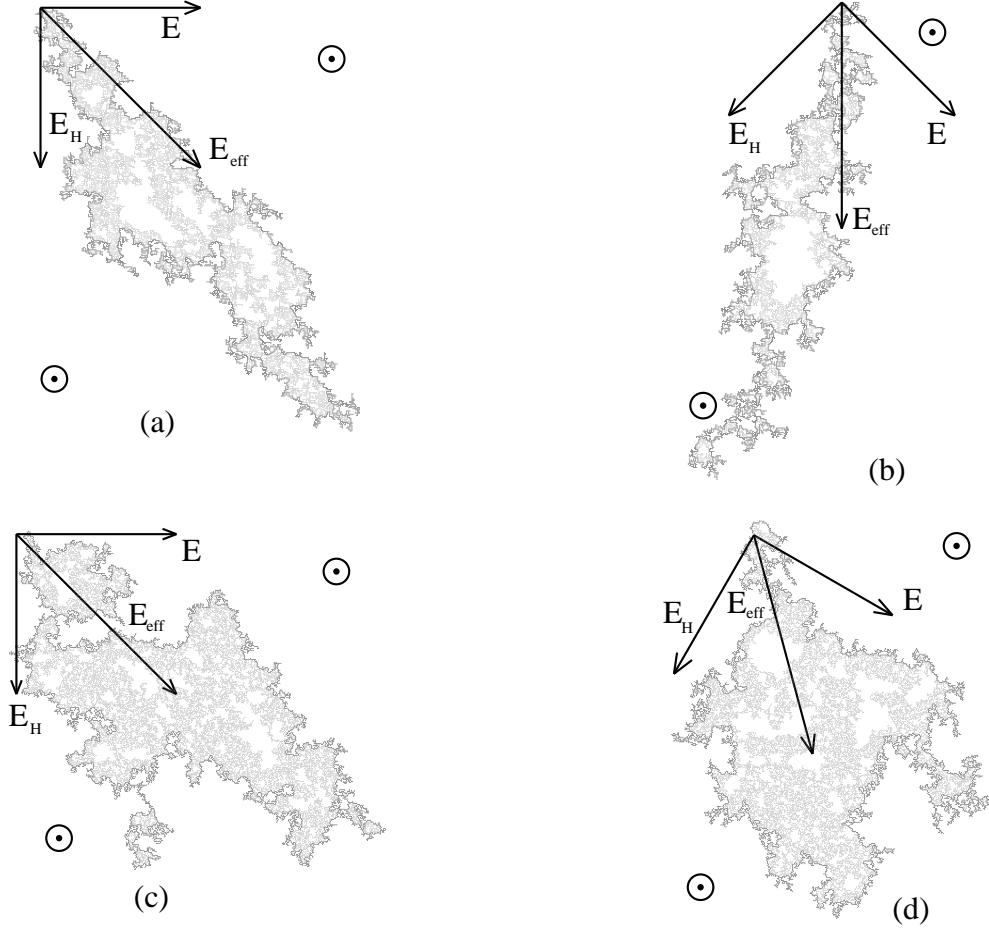


Figure 3: Infinite spanning clusters at  $p = p_c$  on the square (a, b) and triangular (c, d) lattices of size  $L = 2^8$ . For the square lattice, the  $E$  field orientation is horizontal in (a) and it is diagonal in (b). For the triangular lattice, the  $E$  field orientation is horizontal in (c) and it is semi-diagonal (30° with the horizontal) in (d). For all  $E$  field configurations, the  $B$  field is directed into the plane of the lattice. The field lines are drawn from the origin of the clusters.  $E_H$  is the Hall field normal to both  $E$  and  $B$ .  $E_e$  is the resultant field of  $E$  and  $E_H$ . The gray dots represent the interior of the clusters and the black dots represent the cluster hull. The clusters are elongated along the effective field.

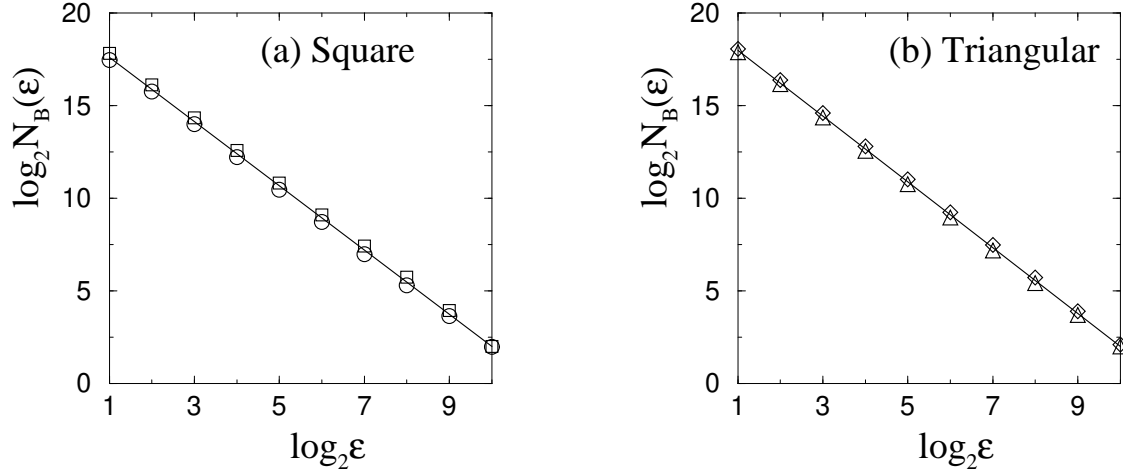


Figure 4: Number of boxes  $N_B(\epsilon)$  is plotted against the box size  $\epsilon$  for the square (a) and triangular (b) lattices to determine the fractal dimension  $d_f$  of the spanning clusters. Squares are for the horizontal  $E$  field and circles are for the diagonal  $E$  field on the square lattice. Triangles are for the horizontal  $E$  field and diamonds are for the semi-diagonal  $E$  field on the triangular lattice. The solid lines are guide to eye. The values of  $d_f$  are obtained as  $d_f = 1.732 \pm 0.006$  for diagonal  $E$  field on the square lattice and  $d_f = 1.777 \pm 0.005$  for the semi-diagonal  $E$  field on the triangular lattice. The value  $d_f$  is then independent of the  $E$  field orientation.

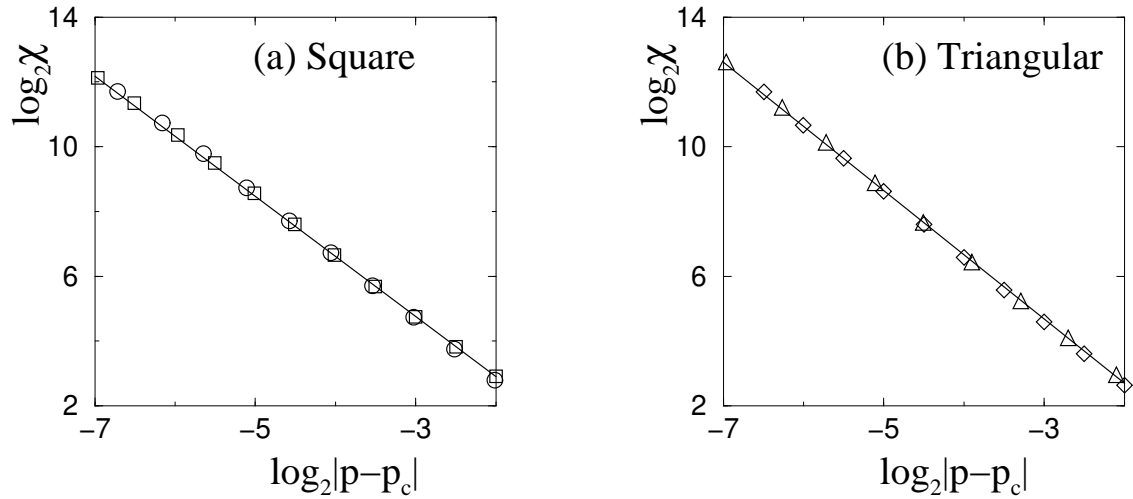


Figure 5: Plot of  $\chi$  against  $|p - p_c|$ : (a) on the square and (b) on the triangular lattice for different  $E$  field configurations. The same symbol set of the previous figure is used. The solid lines are fitted to the data corresponding to the diagonal  $E$  field with slope  $1.87 \pm 0.01$  on the square lattice in (a) and to the semi-diagonal  $E$  field with slope  $2.00 \pm 0.02$  on the triangular lattice in (b).

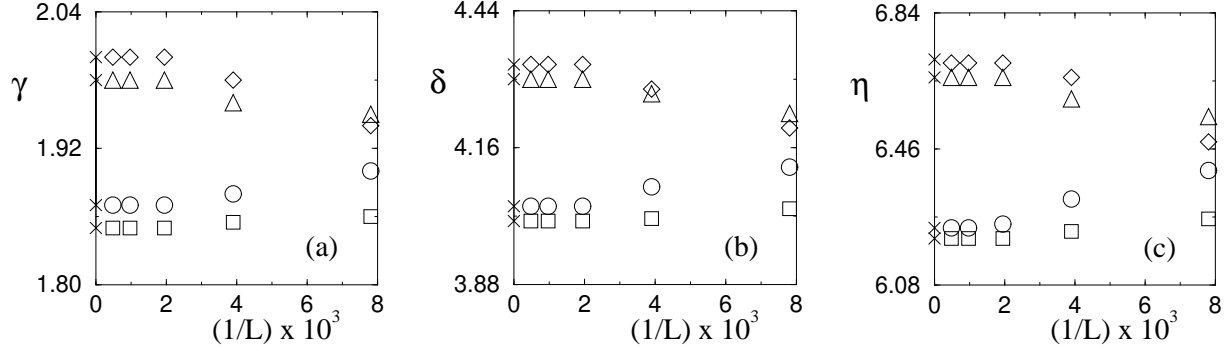


Figure 6: Plot of (a)  $\gamma$ , (b)  $\delta$  and (c)  $\eta$  against  $1/L$  on the square (2, 2) and triangular (4, 3) lattices for different field configurations. The extrapolated values of the exponents are:  $\gamma = 1.85$  and  $1.87$ ,  $\delta = 4.01$  and  $4.04$  and  $\eta = 6.21$  and  $6.24$  for horizontal and diagonal field on the square lattice. On the triangular lattice, the values are:  $\gamma = 1.98$  and  $2.00$ ,  $\delta = 4.30$  and  $4.33$  and  $\eta = 6.66$  and  $6.71$  for the horizontal and semi-diagonal fields. The values of the critical exponents are within error bars for different field orientations.

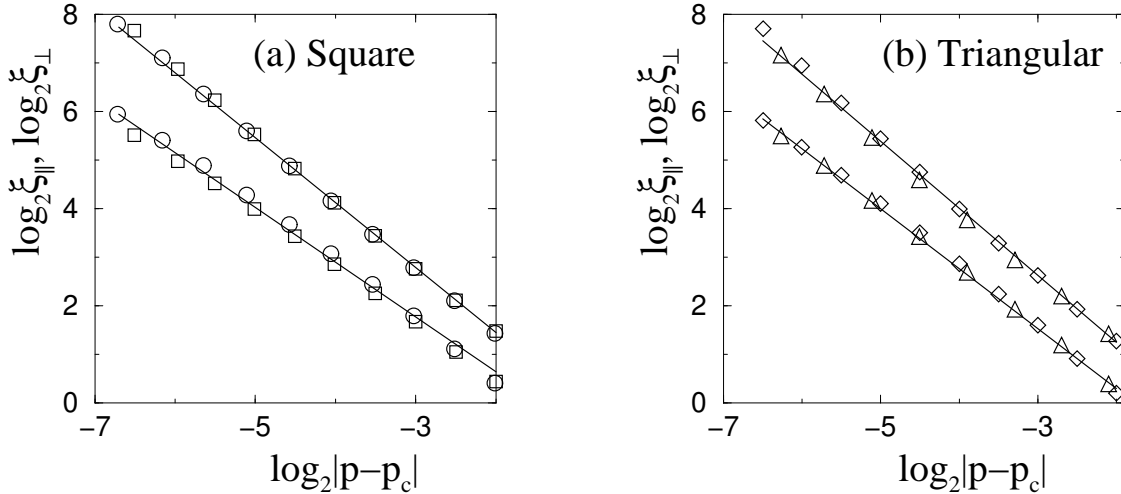


Figure 7: Plot of  $\xi_{\parallel}$  and  $\xi_{\perp}$  against  $|p - p_c|$ : (a) on the square and (b) on the triangular lattice. The same symbol set of Fig. 5 is used for different fields. The values of  $\xi_{\parallel}$  and  $\xi_{\perp}$  are found within error bars for different field orientations.

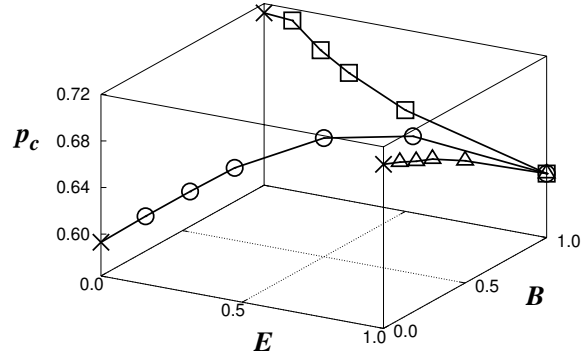


Figure 8: Plot of percolation threshold  $p_c$  against field intensities  $E$  and  $B$  for a square lattice of size  $L = 1024$ . For appropriate values of  $E$  and  $B$ ,  $p_c$ s correspond to that of respective percolation models.

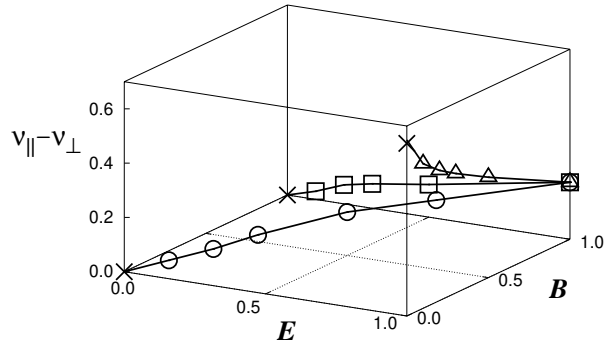


Figure 9: Plot of  $\nu_{||} - \nu_{\perp}$  against field intensities  $E$  and  $B$ .  $\nu_{||} - \nu_{\perp}$  continuously goes to zero as the field intensities goes to  $E = B = 0$  for OP and  $B = 1, E = 0$  for SP respectively.  $\nu_{||} - \nu_{\perp}$  is also approaching 0.64 corresponding to DP for  $E = 1$  and  $B = 0$ .

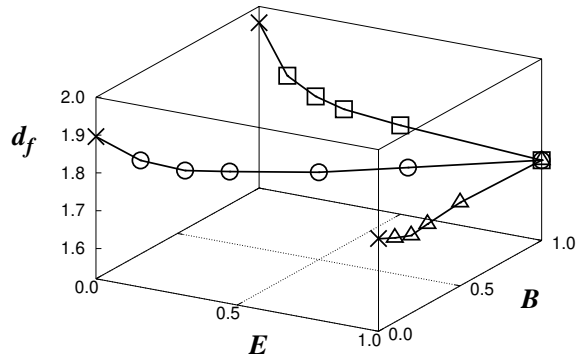


Figure 10: Plot of fractal dimension  $d_f$  of the spanning clusters against field intensities  $E$  and  $B$ . As  $E$  and  $B$  change continuously, the value of  $d_f$  approaches to that of the respective percolation models at the appropriate values of  $E$  and  $B$ .

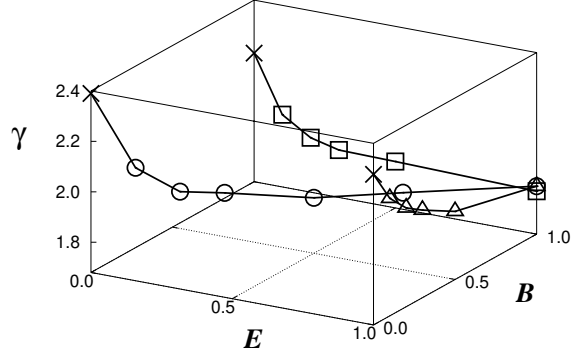


Figure 11: Plot of average cluster size exponent against field intensities  $E$  and  $B$ .  $\gamma$  changes continuously to that of the respective percolation models at the appropriate values of  $E$  and  $B$ .

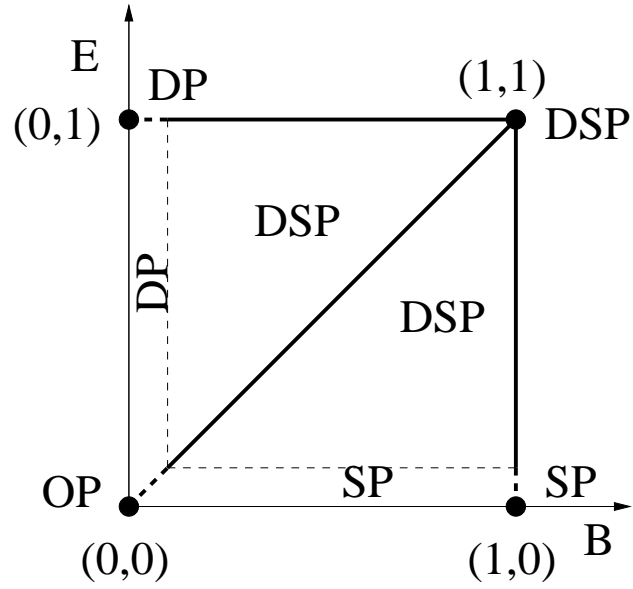


Figure 12: Phase diagram of the percolation models under crossed external bias fields. Different percolation models are represented by black circles. DSP changes continuously to OP, DP or SP for the field intensities of  $E$  and  $B$  are changed to the appropriate values.